Journal of Physics: Conference Series

PAPER • OPEN ACCESS

Impact of rotor size on the aeroelastic behavior of large turbines: a LES study using flexible actuator lines

To cite this article: François Trigaux *et al* 2024 *J. Phys.: Conf. Ser.* **2767** 022062

Journal of Physics: Conference Series **2767** (2024) 022062 doi:10.1088/1742-6596/2767/2/022062

Impact of rotor size on the aeroelastic behavior of large turbines: a LES study using flexible actuator lines

François Trigaux, Philippe Chatelain and Grégoire Winckelmans

Institute of Mechanics, Materials and Civil Engineering (iMMC), Université catholique de Louvain (UCLouvain), 1348 Louvain-la-Neuve, Belgium

E-mail: `francois.trigaux@uclouvain.be`

Abstract. This paper investigates the impact of rotor size on the structural displacements and loads of large wind turbines during power production. The actuator line method is used in Large Eddy Simulations and is coupled to a structural solver for the blades. The latter consists either of a linear solver based on the Euler-Bernoulli beam theory, or uses BeamDyn to account for the non-linearities. The effects of upscaling are investigated for three reference wind turbines of various sizes: the NREL-5 MW, the DTU-10 MW and the IEA-15 MW. The study reveals that the larger turbines exhibit higher bending relative to the radius and a significant torsion angle. The torsion angle is primarily linked to the structural non-linearities and substantially affects the mean blade loads of the largest turbines. Consequently, the power and thrust coefficients predicted using the linear structural model differ from those obtained using BeamDyn. However, the variations of the root bending moments are predicted similarly using both structural solvers; also suggesting that a linear structural solver is still sufficient for the fatigue analysis. Finally, the fatigue analysis is extended to the shaft loads due to the entire rotor, and empirical scaling trends are derived.

1. Introduction

The upscaling of wind turbines has been an important trend over the years and is one of the major contributors to the decrease of the levelized cost of wind energy. However, this cost reduction is only achieved if the turbines remain reliable, thereby keeping the operational expenditures to a moderate level. Therefore, a detailed understanding of the effects of upscaling is essential, particularly concerning the fatigue loads that are a key factor for the lifetime.

Several factors influence the aeroelastic behavior of a wind turbine when the rotor size is increased. First, the characteristics of the wind, such as the wind shear or turbulence, impact the rotor differently. In particular, the ratio between the integral length scale L of the turbulent fluctuations and the rotor diameter D decreases, potentially leading to an increase of the fatigue loads [1, 2]. Second, the larger deformations of the rotors modify the aerodynamics of the blades by adding curvature and sweep [3]. Finally, the rotor structural parameters are modified to limit the mass of the blades, resulting in slender and more flexible blades that exhibit large displacements. These modifications lead to changes in the blade and shaft loads characteristics, that can be challenging to model using traditional approaches, such as the Blade Element Momentum (BEM) theory [1] or linear structural solvers [4, 5].

Journal of Physics: Conference Series **2767** (2024) 022062 doi:10.1088/1742-6596/2767/2/022062

The objectives of this study are first to quantify the evolution of the dynamic response of the rotor with respect to its size. The approach used here is similar to that presented in Pagamonci *et al.* [6]: the structural displacements and their effects on the loads are evaluated for reference wind turbines of different sizes. The originality of this study is the particular attention given to the fatigue loads acting on the blade root and on the rotor shaft. The latter are obtained by leveraging the ability of the LES to accurately capture the turbulence in the flow. Additionally, Pagamonci *et al.* [6] uses a linear structural solver, which does not take the torsion angle into account. In this work, the importance of the structural non-linearities and its evolution with the rotor size is assessed. This is achieved by comparing the results obtained with a linear structural solver to those obtained using the geometrically exact beam theory, especially for the fatigue loads. This analysis focuses on loads encountered during the power production phase, especially near the rated operating conditions, as these usually exhibit the largest structural displacements. The next section presents the methodology, and some results are shown in the second part.

2. Methodology

We perform aeroelastic simulations of three reference wind turbines of different sizes: The NREL-5 MW [7], DTU-10 MW [8] and IEA-15 MW [9] turbines. Some key parameters for these turbines are shown in Table 1. The simulation tool consists in a flexible actuator line method (ALM) implemented in a Large Eddy Simulation (LES) solver, and coupled to a structural solver, as described below.

2.1. Flow solver and actuator line method

The LES of turbulent flow is performed using a 4th order finite difference code [10, 11] on a cartesian staggered grid. The sub-grid scale (SGS) model is a regularized variational multiscale model [12]. The time-integration is performed using a second order Adams-Bashforth scheme. The ALM is used to compute the aerodynamic loads and to model the effect of the blades on the flow [13]. An advanced version of the ALM is used, as described in [14, 15]: its particularity is to use a 2D Gaussian kernel for the velocity sampling and the forces distribution, which provides a better estimation of the aerodynamic forces near the blade tip, compared to using classical 3D Gaussian kernels [16, 17]. No additional near tip correction method is used in the presented simulations.

2.2. Structural solvers

The ALM is also coupled to a structural solver that provides the position, deformations, velocities and internal moment of the blades. Two different structural solvers are compared in this study. The first one is an in-house linear structural solver based on the Euler-Bernoulli beam theory (EB): it uses finite element with linear shape functions for the traction and torsion, and cubic shape functions for the bending (e.g., [18]). It does not account for the blade initial curvature (i.e., the blade pre-bend) in the structural dynamics. In this case, the traction, torsion and bending are decoupled. To include the geometric non-linearities related to large displacements and fully populated 6×6 cross-section matrices, a second structural solver, BeamDyn (BD) [19] is used. The latter solves the equations resulting from the geometrically exact beam theory using high order spectral elements. A comparison of the two structural solvers is provided in section 3.2.

The coupling between the ALM and the structural solver is achieved using a second order improved staggered scheme [20]. The latter evaluates the aerodynamic forces on the ALM at a different time-level than the structural states to improve the accuracy and stability of the coupling. A detailed explanation of the coupling procedure is provided in [15], and a verification in uniform and turbulent flow is provided in [21].

Table 1. Summary of the wind turbines characteristics

	NREL-5 MW	DTU-10 MW	IEA-15 MW
Diameter D [m]	126	178.3	240
Hub height H [m]	90	119	150
Rated wind speed [m/s]	11.4	11.4	10.6
Optimal TSR	7.55	7.5	9
Blade mass [t]	17.5	41.7	65.0

2.3. Numerical set-up and inflow
The turbines are simulated in a domain of size $12D$ in the streamwise direction and $6D$ in the lateral directions, where D is the turbine diameter. Slip conditions are prescribed at the top and bottom of the domain, whereas periodic conditions are used in the transverse direction. The turbine is placed at a distance $3D$ from the inlet and from the lateral boundaries, and the center of the rotor is placed at the prescribed hub height H. The spatial resolution of the flow solver in the vicinity of the wind turbines is 64 grid points per D. The mesh is slightly stretched near the lateral and upper boundaries to reduce the computational cost. As a result, the total number of grid points is $768 \times 256 \times 256$.

The inflow consists of a power law velocity $u/U_{\mathrm{hub}} = (y/H)^{\alpha}$, where y is the vertical coordinate, U_{hub} the velocity at the hub height H and $\alpha = 0.14$ the shear parameter. The inflow hub velocity is set to $U_{\mathrm{hub}} = 9$ m/s, so that the three turbines operate in similar close-to-rated conditions, which corresponds to 79% of the rated velocity for the 5 and 10 MW turbines, and 85% for the 15 MW turbine. Turbulent fluctuations, generated using the Mann algorithm, are also superposed to the inflow [22]. The turbulent length scale is set to $L = 53.1$ m, the anisotropy parameter to $\Gamma = 3.9$, and the $\alpha\epsilon^{2/3}$ parameter is scaled to achieve a turbulence intensity (TI) of 6%. The size of the $3D$ periodic domain in which the turbulent fluctuations are created is 3000 m in the streamwise direction (1024 grid points) and 504 m in the lateral directions (256 grid points). This resolution corresponds to 64 points per diameter for the smallest turbine, which is sufficient to reach convergence of the fatigue loads, according to [23]. To ease the comparison between the turbines, the same turbulence field is used for all turbines, without spatial rescaling. This means that the integral length scale of the turbulence is the same for all the turbines, which is consistent with the IEC standards [24]. The center of the turbulence domain is aligned with the hub of each turbine.

It should be noted that the use of a single hub velocity U_{hub} for all three turbines results in slightly different operating conditions compared to the rated speed. However, it allows for an easier comparison since the turbulent fluctuations are then convected at the same speed for all turbines. Also, the use of a power law velocity profile is more realistic than a linearly sheared profile, but results in slightly different top and bottom inflow speeds for each turbine. Finally, this analysis is limited to one operating point, which corresponds to a close-to-rated condition.

3. Results
3.1. Effect of the upscaling on the displacements and loads
The effect of upscaling is first assessed by simulating the three turbines at a constant rotation speed. The latter corresponds to the turbine optimal TSR, based on the 9 m/s hub velocity. A total of 125 rotations are simulated for each turbine, and the first 25 are removed from the analysis to ensure convergence of the loads. The time-step size of the flow simulation is set to obtain 360 time-steps per rotation. BeamDyn is first used as structural solver and it performs four sub-steps per flow time-steps to ensure a sufficient time discretisation.

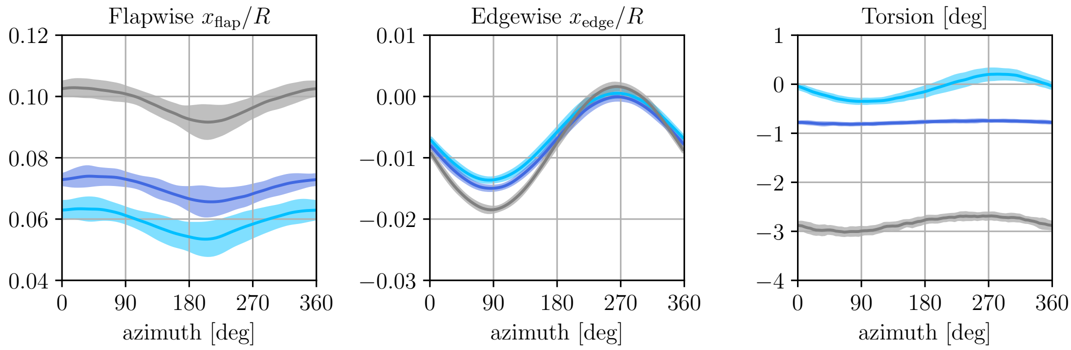

Figure 1. Blade tip displacement as a function of the azimuthal angle for the NREL-5 MW (light blue), DTU-10 MW (dark blue) and IEA-15 MW (gray) turbines, averaged over 100 rotations. The envelope depicts the standard deviation at each angle (0° denotes the blade upward position, which then rotates clockwise).

The blade tip displacements in the flapwise and edgewise directions, along with the torsion angle, are shown in Figure 1 for each turbine. The larger turbines present a higher flapwise deflection relative to their radius: 6.1% for the NREL-5 MW, 7.2% for the DTU-10 MW and 10% for the IEA-15 MW. This is a direct consequence of the lower bending stiffness of the blades. All turbines reach their maximal displacement between 0° and 45° (0° being the upwards position), due to the mean shear of the flow. The maximal standard deviation occurs when the blade is near its downward position. The flapwise displacements have the same phase, but the amplitude of the variation, measured as $(x_{\mathrm{flap,max}} - x_{\mathrm{flap,min}})/\bar{x}_{\mathrm{flap}}$ decreases with the turbine size: 17% for the 5 MW, 12% for the 10 MW and 11% for the 15 MW turbines. The edgewise deformation is mostly sinusoidal, and the standard deviation is very low, due to the dominance of the gravity loads over the aerodynamic loads. The mean relative edgewise deformation $\bar{x}_{edge}/R$ slightly increases with the turbine size: 0.68% for the 5 MW, 0.78% for the 10 MW and 0.88% for the 15 MW turbines. Finally, the mean torsion angle significantly increases with the rotor size. The 5 MW turbine has no mean torsion angle, whereas the 10 MW turbine has a tip torsion angle of -0.8° and the 15 MW has -2.8°. The 5 and 15 MW turbines also present a clear periodic variation of the torsion along the rotation; it is also present for the 10 MW turbine, yet to a lesser extent.

The power spectral density (PSD) of the blade root moments is depicted in Figure 2. To facilitate the comparison, the root moments are normalized by their mean value before computing the PSD. These mean moments importantly increase in both directions with the rotor size, and the flapwise moment is one order of magnitude larger than that in the edgewise direction. For all turbines, the dominant frequency of the PSD is the rotation frequency (1P). At this frequency, the PSD reaches a much higher value in the edgewise direction, indicating the importance of the variation of the loads in this direction. This variation is due to the gravity loads that change direction during the rotation of the blade. The peak of the PSD is also slightly higher for the 5 MW turbine in the flapwise direction and slightly lower in the edgewise direction, whereas the 10 and 15 MW turbines essentially present the same value. The first harmonics of the rotation frequency are excited similarly for all turbines. In the flapwise direction, the blade natural frequencies correspond to 4P for the 5 MW turbine, and 5P for the 10 and 15 MW turbines. No particular peak of the PSD is observed at these frequencies, which confirms the high aerodynamic damping of the flapwise modes. On the contrary, clear peaks are noticeable at the edgewise natural frequencies, which correpond to 6P for the 5 and 15 MW turbines, and 8P for the 10 MW turbine. However, the amplitude of these peaks remains small compared to

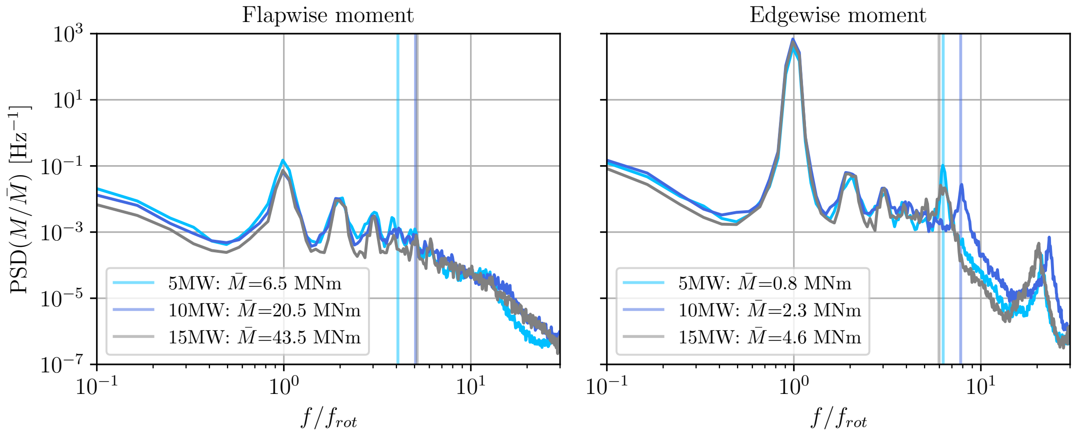

Figure 2. PSD of the flapwise and edgewise root bending moments for the NREL-5 MW (light blue), DTU-10 MW (dark blue) and IEA-15 MW (gray) turbines. The moments are normalized by their time-averaged value $\bar{M}$. For each turbine, the vertical line corresponds to the blade first natural frequency in the considered direction.

that observed at the 1P frequency. Finally, the spectrum tends to be more concentrated around the harmonics of the rotation frequencies for the larger turbines. This is a consequence of both the increased shear of the inflow and the fixed integral length scale of the turbulent inflow [1]. In fact, when the scale of the turbulent fluctuations is smaller than the rotor radius, it leads to a variation of the loads during the rotation, which appears at the 1P frequency and its first harmonics. On the contrary, larger scales impact the entire rotor, leading to load variations that mostly appear in the lower frequencies and that are less detrimental for the fatigue [2].

3.2. Impact of the structural non-linearities

Having quantified the main effects of the rotor upscaling over the displacement and the blade loads, the importance of the non-linearities is now assessed by comparing the simulations of Section 3.1 to same simulations using the linear structural solver based on the Euler-Bernoulli beam theory (EB).

The time-averaged load distribution is depicted in Figure 3. For the 5 MW turbine, the load distribution predicted by the linear solver is in good agreement with that predicted using BeamDyn. For the 10 and 15 MW turbines, the linear solver predicts higher loads in both the flapwise and edgewise directions on the outer part of the blade. These differences originate from the absence of bend-twist coupling in the linear solver. As a result, the mean torsion predicted by the linear solver is much smaller than that obtained by BeamDyn, which results in an increased angle of attack, and consequently a higher lift.

Due to the forces increase, the aerodynamic properties of the rotor obtained using the EB solver are higher than those obtained using BeamDyn, as denoted in Table 2. While both solvers predict virtually identical thrust and power coefficients for the 5 MW turbine, the predictions for the 10 MW turbine turbines differ by a few percent, and by more than 5% for the 15 MW turbine. Consequently, the linear solver predicts higher flapwise displacement. It also tends to underestimate the mean edgewise displacement, although the aerodynamic forces are higher in that direction. The largest differences are related to the mean torsion angle at the tip, for which the EB solver typically predicts small values, in contrast to the large negative values predicted by BeamDyn. It should also be noted that the reported power coefficients are higher

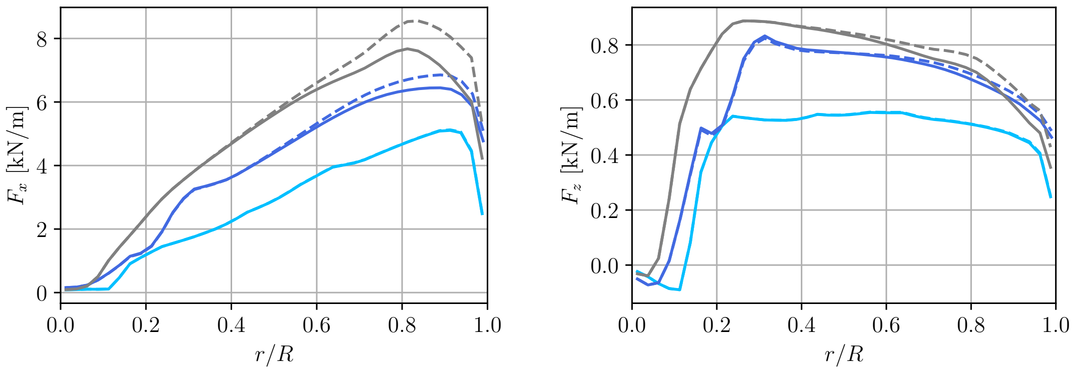

Figure 3. Time-averaged aerodynamic force distribution over the blade in the normal (left) and tangential (right) directions, expressed in the blade root frame. Comparison between the BeamDyn (solid) and EB (dash) solvers.

Table 2. Comparison of the thrust (C_T) and power (C_P) coefficients of the aerodynamic forces, and tip deformation obtained using the BeamDyn and EB solvers.

Turbine	Struct.	C_T		C_P		$\bar{x}_{flap}$ [m]	$\bar{x}_{edge}$ [m]	$\bar{\phi}$ [deg]
NREL-5 MW	BD	0.82		0.55		3.75	-0.41	-0.08
	EB	0.82	(+0.1 %)	0.55	(+0.4 %)	3.77	-0.42	-0.06
DTU-10 MW	BD	0.83		0.54		6.26	-0.67	-0.78
	EB	0.86	(+3.0 %)	0.55	(+1.5 %)	6.25	-0.48	0.18
IEA-15 MW	BD	0.75		0.51		11.79	-1.01	-2.83
	EB	0.80	(+6.5 %)	0.53	(+4.6 %)	12.37	-0.91	-0.72

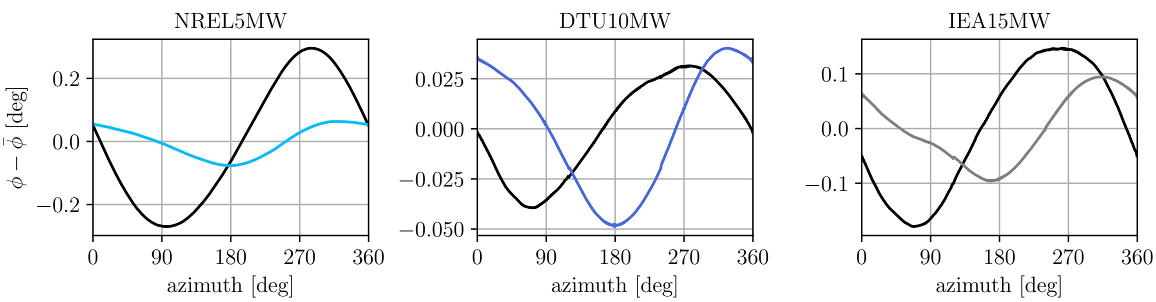

Figure 4. Blade tip torsion angle as a function of the azimuthal angle. Comparison between the BeamDyn (black) and EB (blue) solvers.

than the reported design coefficient of the considered turbines. This is due to the fact that they were designed using a BEM method, whereas the presented simulations use the ALM in a LES framework. In near-rated conditions, the ALM tends to predict higher edgewise forces and therefore a higher power coefficient than that obtained using the BEM (see, e.g., [25, 26, 27, 28, 21]).

Not only is the mean value of the torsion predicted differently, but its variation along the

Table 3. Damage equivalent loads of the blade root moments at 1Hz frequency.

		NREL-5 MW	DTU-10 MW	IEA-15 MW	Scaling
DEL M_{flap} [MNm]	BD	1.90	3.95	7.23	$1.01\,R^{2.06}$
	EB	1.85 (-2.1%)	3.99 (+0.9%)	7.14 (-1.3%)	$1.04\,R^{2.04}$
DEL M_{edge} [MNm]	BD	5.82	17.51	29.13	$1.29\,R^{2.12}$
	EB	5.67 (-2.6%)	16.91 (-3.4%)	27.70 (-4.9%)	$1.29\,R^{2.09}$

rotation also differs in phase. In fact, the period-average of the torsion at the tip, depicted in Figure 4, reveals that the torsion reaches its maximal value when the blade points upwards for the EB solver, whereas it is maximal when the blade is horizontal with BeamDyn. This is due to the absence of coupling between the torsion and the other degrees of freedom in the EB solver. Consequently, the only effect impacting the torsion is the aerodynamic moment. This moment oscillates with the blade height due to the mean shear of the flow, leading to an up-down variation. On the contrary, the BeamDyn model accounts for additional aspects. First, the coupling between the flapwise bending and the torsion in the cross-section stiffness matrices results in a mean torsion value. Second, due to the flapwise bending, the edgewise forces applied on the deformed axis create a torsional moment on the reference axis. The latter alternates with the phase of the edgewise forces, which mostly consist of the gravity loads. The aerodynamic moment plays a much smaller role compared to these effects, resulting in a different phase between the two solvers.

3.3. Fatigue analysis

The fatigue loads resulting from the blade root moments are evaluated in this section. To quantify the total fatigue undergone by a turbine, the damage equivalent loads (DELs) are computed at a frequency of 1 Hz and using $m = 10$ as coefficient for the S-N curve. Note that the DEL only includes the effect of the alternating moment, and not that of the mean moment. The flapwise and edgewise root moments are here measured on 100 turbine rotations, which corresponds to 582, 830 and 931 seconds for the 5, 10 and 15 MW turbines, respectively. The cycle count is performed by applying the rainflow counting algorithm on the three blades and is averaged to represent the damage undergone by one blade.

The DELs computed using the blade root moments provided by the various structral solvers are reported in Table 3. The results obtained by the EB solver and by BeamDyn are presented for comparison. The DELs predicted by the two solvers are very close for each turbine in the flapwise direction. This results from the similar response of the structural solver to the variation of the aerodynamic loads. Although the mean load distribution of the blade differs between the two solvers, the fatigue loads that only account for the alternating moment are therefore virtually identical. In the edgewise direction, the difference between the DEL predicted by the two solvers tends to grow slightly with the rotor size. In general, both solvers predict quite similar DELs, which validates the use of a linear structural solver for fatigue analysis in this case.

The scaling tendency, obtained by fitting a function $f = a\,R^b$ to the DELs of the various turbines, are also predicted similarly by the two structural solvers. The DEL of the flapwise moment increases slightly more slowly with R than that of the edgewise moment. The increase in flapwise moment is dependent on the inflow and particularly on the shear parameter (see [29, 30]), whereas the equivalent edgewise moment depends on the increase in mass of the blades. The DEL in the edgewise direction is initially higher than that in the flapwise direction, and will thus be a dominant factor in the blades design. This is consistent with the current effort to reduce the blade mass.

Table 4. Comparison of the time-averaged rotation speed, thrust and power coefficients, and of the tip deflection, obtained enforcing a constant rotation speed or using the ROSCO controller.

Turbine	Control	$\bar{\Omega}$ [rpm]	C_T	C_P	$\bar{x}_{flap}$	$\bar{x}_{edge}$	$\bar{\phi}$
NREL-5 MW	None	10.30	0.82	0.55	3.75	-0.41	-0.08
	ROSCO	10.82 (+5.1%)	0.85 (+3.2%)	0.57 (+1.8%)	3.82	-0.41	-0.18
DTU-10 MW	None	7.23	0.83	0.54	6.26	-0.67	-0.78
	ROSCO	7.38 (+2.1%)	0.85 (+1.9%)	0.54 (+0.7%)	6.37	-0.67	-0.81
IEA-15 MW	None	6.45	0.75	0.51	11.79	-1.01	-2.83
	ROSCO	6.51 (+1.0%)	0.76 (+0.9%)	0.51 (+0.4%)	11.84	-1.01	-2.90

3.4. Controller and shaft loads

To complete the fatigue analysis, it is recommended to also consider the loads acting on the shaft tip and due to the entire rotor. These include the rotor yaw and tilt moments, the axial thrust and torsion on the shaft [31]. However, the shaft loads cannot be evaluated correctly from a simulation that enforces a constant rotation speed. Indeed, in that case, the rotation of the blade is applied as a kinematic boundary condition at the blade root. This decouples the dynamics of the different blades and of the drivetrain. The simulations presented in this section have therefore been run using the ROSCO controller [32], together with the non-linear structural solver BeamDyn. The coupling between the blades root bending moments and the drivetrain dynamics also requires smaller time-steps to converge, so that the number of structural sub-steps is increased to 10 sub-steps per flow time-steps in the cases that includes the controller.

Table 4 presents the rotor speed, thrust and power coefficients and the displacements obtained with the controller enabled. The time-averaged rotation speed of the rotor is slightly higher than that obtained from the optimal TSR and the hub speed. This results from the combination of two effects. First, the controller uses the C_T and C_P values obtained using the Blade Element Momentum theory (BEM) to estimate the upstream velocity. These are smaller than those obtained using the ALM in similar operating conditions, resulting in an over-estimation of the upstream velocity. On the other hand, the mean wind velocity on the rotor area is slightly slower than the hub speed due to the exponent profile at the inflow. Nevertheless, the rotor thrust and power coefficients obtained with the controller enabled are only marginally higher than those obtained at constant rotation speed. Consequently, the mean flapwise deflection and torsion angle at the tip are also slightly increased, but remain globally consistent with those of the simulation at constant rotation speed.

The changes in blade and shaft loads induced by the addition of the controller are also investigated by comparing their PSD in Figure 5. The PSD of the blade root flapwise moment is not much impacted by the controller. Only the lowest frequencies are affected by its action, due to the variations of the rotation speed that adapts to the inflow variations. The edgewise root moment is more impacted. The lowest frequencies present smaller variations than the case with constant rotation speed, as the controller aims at maintaining the rotor torque constant. The spread around the 1P frequency is larger due to the changes in rotation speed, that affect the frequency at which the gravity loads are applied. Finally, a significant decrease of the PSD at the 3P frequency results from the controller effort to smooth the rotor torque. The most affected load is the torque on the shaft: whereas it is mostly dominated by the 3P and edgewise frequency when the blades have a fixed rotation speed, the coupling to the drivetrain significantly decreases these variations. As a result, the rotor shaft mostly consists of low frequency variations that are imposed by the generator to adapt to the changes in wind speed. The controller has a minimal impact on the axial thrust, the yawing and the tilting moments.

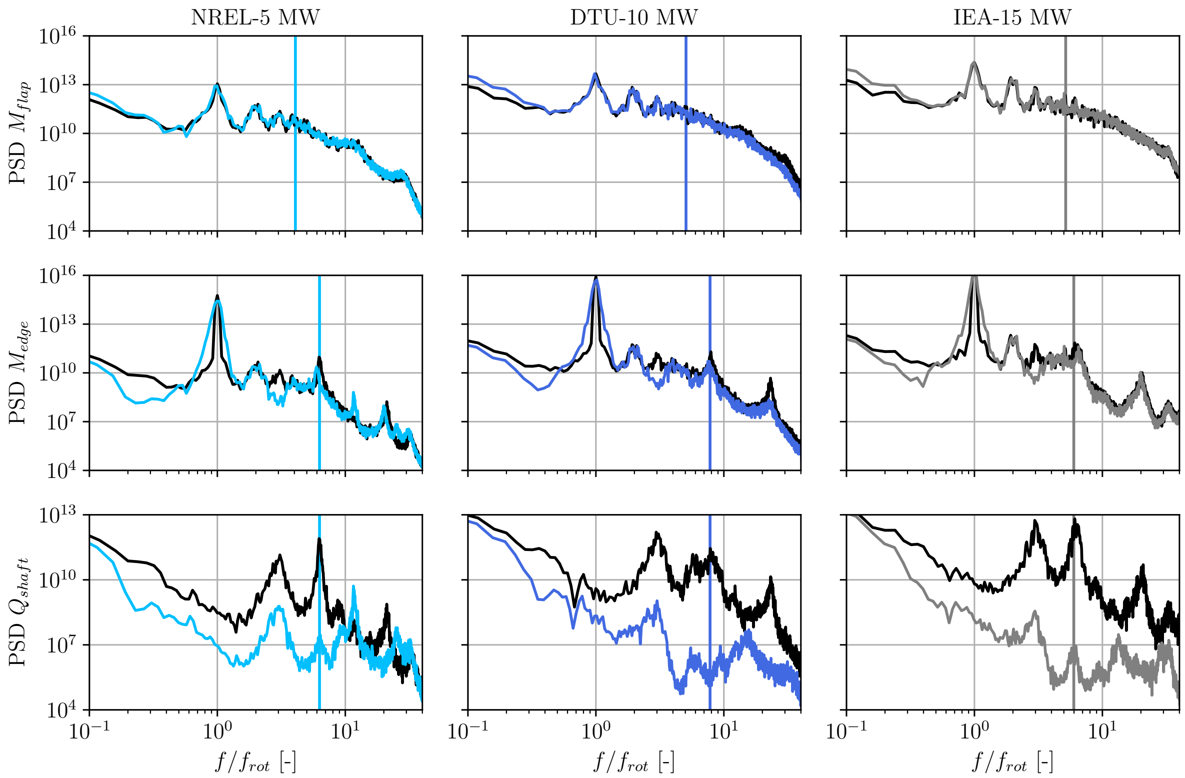

Figure 5. PSD of the blade root flapwise moment (top), blade root edgewise moment (middle) and shaft torque (bottom). Comparison between the results obtained at constant rotation speed (black) and using the ROSCO controller (blue or gray).

Table 5. Damage equivalent loads obtained using the ROSCO controller.

DEL [MNm]	NREL-5 MW	DTU-10 MW	IEA-15 MW	Scaling
Blade flapwise moment	2.215	4.673	7.907	$1.06\,R^{1.90}$
Blade edgewise moment	5.826	17.499	29.119	$1.29\,R^{2.13}$
Shaft torque	0.199	0.353	0.431	$1.11\,R^{1.09}$
Yawing moment	1.082	2.470	4.234	$1.09\,R^{1.99}$
Tilting Moment	1.132	2.518	4.269	$1.08\,R^{1.95}$

Finally, the evolution of the DELs is presented in Table 5. The DELs associated to the flapwise blade root moment are slightly higher than those obtained at a constant rotation speed, mostly due to the increase of the thrust coefficient. Their scaling exponent is also lower than that obtained at a constant rotation speed. This is also related to the change in thrust coefficient, that is more pronounced for the smaller turbine. The DELs are generally constant in the edgewise direction. The torque on the shaft presents a moderate DEL that slightly increases with the rotor size, due to the effect of the controller that decreases importantly the torque variations. The yawing and tilting moment present similar amplitudes and increase similarly with the rotor size.

4. Conclusion

This paper investigates the evolution of the blade and shaft loads as a function of rotor size during the power production. Three reference wind turbines were simulated using an aeroelastic framework based on a flexible actuator line method in Large Eddy Simulations. The advantage of this methodology is that many rotation cycles are simulated, while also accounting for the effect of the inflow turbulence, which allows to conduct a fatigue analysis. This investigation leads to the following conclusions:

- The flapwise deformation relative to the rotor radius increases with the turbine rated power, reaching 10% for the largest turbine. The larger turbines also exhibit a non-negligible mean torsion angle that influences the aerodynamics of the blades.
- For all turbines, the blade root moments vary mostly at the 1P frequency due to the mean shear of the flow and the gravity loads. The moments at the root of the larger turbines also have their spectrum more concentrated around the rotation frequency due to the higher mean shear of the inflow and the smaller size of the turbulent scales relative to the rotor size.
- Fatigue loads on the blades have a larger amplitude in the edgewise direction due to the gravity than in the flapwise direction due to the inflow shear. Moreover, they increase faster with the rotor radius in the edgewise direction than in the flapwise direction.

Considering the increase in magnitude of the relative displacement, the influence of the geometric non-linearities on the structural dynamics is also assessed by comparing the results obtained with two structural solvers: a linear one (Euler-Bernoulli beam) and a non-linear one (BeamDyn, also with bend-twist coupling). The largest discrepancies are related to the modeling of the torsion, whose mean value and phase are predicted differently. This has a significant impact on the mean load distribution over the blades of the larger turbines. However, the two structural solvers predict a similar variation of the blade root moment, leading to a consistent fatigue load evaluation.

Lastly, modeling the controller is shown to primarily affect the blade edgewise moment and the torque on the rotor shaft. The impact on the blade flapwise moment and on the rotor yawing and tilting moments is minimal. The damage equivalent loads of the blade root moments and yawing and tilting moments are found to scale as $\simeq R^{1.9-2.1}$, with the edgewise blade root moment consistently presenting the highest exponent.

Acknowledgments

The funding for this research was provided by the Belgian Energy Transition Fund in the framework of the PhairywinD project. This research benefited from computational resources made available on the Tier-1 supercomputer of the Fédération Wallonie-Bruxelles, infrastructure funded by the Walloon Region under the grant agreement No. 1117545. Computational resources were also provided by the Consortium des Equipements de Calcul Intensif (CECI), funded by the Fonds de la Recherche Scientifique de Belgique under Grant No. 2.5020.11 and by the Walloon Region.

References

[1] Madsen H A, Larsen T J, Pirrung G R, Li A and Zahle F 2020 *Wind Energy Science* **5** 1–27
[2] Dimitrov N, Natarajan A and Mann J 2017 *Renewable Energy* **101** 1180–1193
[3] Fritz E K, Ferreira C and Boorsma K 2022 *Wind Energy* **25** 1977–1994
[4] Riziotis V, Voutsinas S, Politis E, Chaviaropoulos P, Hansen A M, Madsen H and Rasmussen F 2008 *Proceedings of the EWEC* vol 8
[5] Manolas D, Riziotis V and Voutsinas S 2015 *Journal of Computational and Nonlinear Dynamics* **10** 041008
[6] Pagamonci L, Papi F, Balduzzi F, Xie S, Sadique J, Scienza P and Bianchini A 2023 *Journal of Physics: Conference Series* vol 2648 (IOP Publishing) p 012005

[7] Jonkman J, Butterfield S, Musial W and Scott G 2009 Definition of a 5-mw reference wind turbine for offshore system development Tech. rep. National Renewable Energy Lab.(NREL), Golden, CO (United States)
[8] Bak C, Zahle F, Bitsche R, Kim T, Yde A, Henriksen L C, Hansen M H, Blasques J P A A, Gaunaa M and Natarajan A 2013 *Danish wind power research 2013*
[9] Gaertner E, Rinker J, Sethuraman L, Zahle F, Anderson B, Barter G E, Abbas N J, Meng F, Bortolotti P, Skrzypinski W *et al.* 2020 Iea wind tcp task 37: definition of the iea 15-megawatt offshore reference wind turbine Tech. rep. National Renewable Energy Lab.(NREL), Golden, CO (United States)
[10] Duponcheel M, Bricteux L, Manconi M, Winckelmans G and Bartosiewicz Y 2014 *International Journal of Heat and Mass Transfer* **75** 470 – 482
[11] Moens M 2018 Large eddy simulation of wind farm flows: improved actuator disk model and investigation of wake phenomena phD thesis at Université Catholique de Louvain
[12] Jeanmart H and Winckelmans G 2002 *Proceedings of the summer program* pp 105–116
[13] Sorensen J N and Shen W Z 2002 *Journal of Fluids Engineering* **124** 393–399
[14] Trigaux F, Chatelain P and Winckelmans G 2022 *Journal of Physics: Conference Series* vol 2265 (IOP Publishing) p 022050
[15] Trigaux F, Chatelain P and Winckelmans G 2023 *Journal of Physics: Conference Series* vol 2505 (IOP Publishing) p 012034
[16] Jha P K and Schmitz S 2018 *Journal of Fluid Mechanics* **834** R2
[17] Caprace D G, Chatelain P and Winckelmans G 2019 *AIAA Journal* **57** 17–28
[18] Neto M A, Amaro A, Roseiro L, Cirne J and Leal R 2015 *Engineering computation of structures: the finite element method* (Springer)
[19] Wang Q and Yu W 2017 *Journal of Renewable and Sustainable Energy* **9** 033306
[20] Degroote J 2013 *Archives of computational methods in engineering* **20** 185–238
[21] Trigaux F, Chatelain P and Winckelmans G 2024 *Wind Energy Science Discussions* **2024** 1–33
[22] Mann J 1998 *Probabilistic engineering mechanics* **13** 269–282
[23] Liew J and Larsen G C 2022 *Journal of Physics: Conference Series* vol 2265 (IOP Publishing) p 032049
[24] IEC 2005 *International Standard IEC61400-1: Wind Turbinese Part 1 : Design Guidelines*
[25] Madsen H A, Riziotis V, Zahle F, Hansen M O L, Snel H, Grasso F, Larsen T J, Politis E and Rasmussen F 2012 *Wind Energy* **15** 63–81
[26] Perez-Becker S, Papi F, Saverin J, Marten D, Bianchini A and Paschereit C O 2020 *Wind Energy Science* **5** 721–743
[27] Shaler K, Anderson B, Martínez-Tossas L A, Branlard E and Johnson N 2023 *Wind Energy Science* **8** 383–399
[28] Sayed M, Lutz T, Krämer E, Shayegan S and Wüchner R 2019 *Journal of Fluids and Structures* **87** 354–377 ISSN 0889-9746
[29] Park J, Basu S and Manuel L 2014 *Wind Energy* **17** 359–384
[30] Dimitrov N, Natarajan A and Kelly M 2015 *Wind Energy* **18** 1917–1931
[31] Hansen M 2008 *Aerodynamics of Wind Turbines* 2nd ed (Earthscan)
[32] Abbas N J, Zalkind D S, Pao L and Wright A 2022 *Wind Energy Science* **7** 53–73